Comparisons of Satellite-Derived Atmospheric Motion Vectors, Rawinsondes, and NOAA Wind Profiler Observations

KRISTOPHER M. BEDKA, CHRISTOPHER S. VELDEN, RALPH A. PETERSEN,
AND WAYNE F. FELTZ

*Cooperative Institute for Meteorological Satellite Studies, University of Wisconsin—Madison,
Madison, Wisconsin*

JOHN R. MECIKALSKI

Atmospheric Sciences Department, University of Alabama in Huntsville, Huntsville, Alabama

ABSTRACT

Geostationary satellite-derived atmospheric motion vectors (AMVs) have been used over several decades in a wide variety of meteorological applications. The ever-increasing horizontal and vertical resolution of numerical weather prediction models puts a greater demand on satellite-derived wind products to monitor flow accurately at smaller scales and higher temporal resolution. The focus of this paper is to evaluate the accuracy and potential applications of a newly developed experimental mesoscale AMV product derived from Geostationary Operational Environmental Satellite (GOES) imagery. The mesoscale AMV product is derived through a variant on processing methods used within the University of Wisconsin—Madison Cooperative Institute for Meteorological Satellite Studies (UW-CIMSS) AMV algorithm and features a significant increase in vector density throughout the troposphere and lower stratosphere over current NOAA/ National Environmental Satellite, Data, and Information Service (NESDIS) processing methods for *GOES-12* Imager data. The primary objectives of this paper are to 1) highlight applications of experimental GOES mesoscale AMVs toward weather diagnosis and forecasting, 2) compare the coverage and accuracy of mesoscale AMVs with the NOAA/NESDIS operational AMV product, and 3) demonstrate the utility of 6-min NOAA Wind Profiler Network observations for satellite-derived AMV validation. Although the more conservative NOAA/NESDIS AMV product exhibits closer statistical agreement to rawinsonde and wind profiler observations than do the experimental mesoscale AMVs, a comparison of these two products for selected events shows that the mesoscale product better depicts the circulation center of a midlatitude cyclone, boundary layer confluence patterns, and a narrow low-level jet that is well correlated with subsequent severe thunderstorm development. Thus, while the individual experimental mesoscale AMVs may sacrifice some absolute accuracy, they show promise in providing greater temporal and spatial flow detail that can benefit diagnosis of upper-air flow patterns in near–real time. The results also show good agreement between 6-min wind profiler and rawinsonde observations within the 700–200-hPa layer, with larger differences in the stratosphere, near the mean top of the planetary boundary layer, and just above the earth's surface. Despite these larger differences within select layers, the stability of the difference profile with height builds confidence in the use of 6-min, ~404-MHz NOAA Wind Profiler Network observations to evaluate and better understand satellite AMV error characteristics.

1. Introduction

For several decades, atmospheric motions deduced from sequential multispectral geostationary satellite imagery have been commonly used by forecasters to help define flow fields and weather system development. With advances in computing power and satellite instrumentation technology, the spatial coverage, accuracy, and detail of the flows depicted from satellites have improved dramatically from the 1960s (Fujita et al. 1969) to the present (Velden et al. 2005). Objectively determined atmospheric motion vectors (AMVs) have been previously described within a wide variety of meteorological

Corresponding author address: Kristopher M. Bedka, Cooperative Institute for Meteorological Satellite Studies, University of Wisconsin—Madison, 1225 West Dayton St., Madison, WI 53706. E-mail: kristopher.bedka@ssec.wisc.edu

applications, such as NWP model data assimilation (Goerss et al. 1998; LeMarshall et al. 1996; Leslie et al. 1998; Xiao et al. 2002; Kelly et al. 2004), convective weather forecasting (Negri and Vonder Haar 1980; Rabin et al. 2004; Mecikalski and Bedka 2006), and tropical cyclone forecasting (Rodgers and Gentry 1983; Velden et al. 1992; Dunion and Velden 2002).

Operational satellite data processing centers in the United States, Europe, Asia, and Australia routinely produce geostationary AMV datasets several times during each day for the latitude band extending from approximately 60°S to 60°N. Processing of these datasets has been primarily directed toward depiction of larger-scale flow fields with reasonable accuracy for input into global numerical models. However, current and future generation regional mesoscale modeling efforts are beginning to place an increasing demand on accurate satellite-derived products to depict flow variability at smaller scales and higher temporal resolution. Our ability to meet this demand is governed by the spatial, temporal, and spectral resolution of improving satellite instrumentation, as well as assumptions and settings inherent to automated AMV algorithms.

Bedka and Mecikalski (2005, hereinafter referred to as BM05) introduced a new AMV processing methodology that extends the current operational National Oceanic and Atmospheric Administration/National Environmental Satellite, Data, and Information Service (NOAA/NESDIS) automated algorithm toward depiction of mesoscale flows and their local variability. This experimental mesoscale AMV processing methodology was designed to track cloud and water vapor (WV) features associated with convective clouds at multiple levels within the troposphere, and includes an adjustment of quality-control procedures to allow for significant deviation from an NWP-based background wind analysis. BM05 demonstrated these so-called mesoscale AMVs within an algorithm that computes cumulus cloud-top cooling rates, but did not quantitatively assess the relative accuracy of the AMV field.

The objectives of this study are 1) to demonstrate the potential utility of the mesoscale AMV fields for qualitative diagnosis of upper-air flow patterns, 2) to quantify their accuracy relative to collocated rawinsonde and 6-min NOAA 404-MHz wind profiler observations near the U.S. Department of Energy (DOE) Atmospheric Radiation Measurement (ARM) Program Southern Great Plains (SGP) Central Facility at Lamont, Oklahoma, and 3) to demonstrate the utility of 6-min NOAA Wind Profiler Network observations for satellite-derived AMV validation.

Section 2 provides background information on past efforts to extract mesoscale flow patterns from satellite,

in addition to a description of issues associated with AMV validation. Section 3 highlights the qualitative application of mesoscale AMVs to weather diagnosis and forecasting. Section 4 describes the validation datasets and methodology. Section 5 presents comparisons between winds derived from collocated AMVs, wind profiler, and rawinsonde. Section 6 provides a discussion on the study results. Section 7 summarizes the findings.

2. Background

a. Satellite-derived mesoscale flow identification

Current-generation AMV algorithms determine the quality of their satellite-derived wind fields by measuring both the spatial and temporal coherency of a given vector [quality indicator (QI) analysis; Holmlund 1998] and the agreement with an NWP model–based "first guess" background wind analysis (recursive filter analysis; Hayden and Purser 1995). These scores are then used to decide whether or not a given vector is included in the final operational AMV data. This is done to assure that the AMVs represent large-scale flow and therefore are more likely to be preserved during NWP data assimilation. However, in situations with complex mesoscale flows, vectors that may accurately depict the conditions present at the smallest scales can be rejected by these quality-control algorithms because the satellite flow greatly deviates from that represented by the often coarse horizontal resolution background analysis.

Rabin et al. (2004) demonstrate the impact of reducing the required AMV-background wind field agreement for *Geostationary Operational Environmental Satellite* (*GOES*)-*8* water WV AMVs (Velden et al. 2005). They were able to capture upper-level divergence and vorticity patterns with temporal and spatial resolution superior to that possible from NOAA/NESDIS operational AMV datasets (OPER hereinafter) and other observational sources. The divergence and vorticity fields were shown to be quite useful in diagnosing areas of upper-tropospheric vertical motion, which can aid in forecasting future locations of convective storm development.

In the development of their experimental mesoscale AMV product (MESO hereinafter), BM05 further adjust the AMV algorithm processing methods described by Rabin et al. (2004) in that BM05 acquire MESO from 1-km visible (VIS) and 4-km infrared (IR) window imagery in addition to the water vapor imagery used by Rabin et al. The MESO processing scheme represents a variant of the OPER algorithm processing settings but greatly increases the vector density that can be derived from the current *GOES-12* Imager throughout the troposphere and lower stratosphere. Major changes include

TABLE 1. A summary of the primary differences in processing settings between MESO and OPER.

AMV algorithm parameter	MESO setting	OPER setting
Target box size	5×5 pixels ($\sim$25 km^2 for VIS and $\sim$400 km^2 for IR and WV)	15×15 pixels ($\sim$225 km^2 for VIS and $\sim$3600 km^2 for IR and WV)
VIS AMV height range	1000–100 hPa	1000–600 hPa
Min allowed recursive filter analysis score	0.01	0.50
Min allowed QI score	0.50	0.60
Gross speed and directional comparison with NWP forecast	No	Yes
Max IR window target temperature	285 K	250 K

a reduction in both the required AMV agreement with an NWP-based background wind analysis and the size of target boxes that are tracked by the algorithm. Targets in the VIS channel are also tracked up to the 100-hPa level, providing high-density flow information from cirrus clouds and convective storm outflow. A complete summary of the primary differences between BM05, MESO, and OPER processing is provided in Table 1.

The MESO product was developed as a means of tracking clouds to monitor infrared cloud-top growth rates for individual cumulus clouds in near–real time as part of a convective storm initiation nowcast system (Mecikalski and Bedka 2006). MESO are used to identify the past locations of cumuliform cloud pixels without concern for AMV accuracy relative to a ground-based truth wind measurement. A convective cloud mask is used to verify whether a predicted past pixel contains a cumulus, thereby mitigating the impact of grossly errant AMVs that could induce false alarms in their cloud-top growth rate product.

BM05 show that their processing methodology increases the number of vectors by a factor of 20 over OPER for a severe thunderstorm event over the U.S. southern plains. These vectors depicted flow regimes associated with convective cloud-top outflow, midtropospheric divergence, and convergence within a convective boundary layer at significantly greater detail than vectors from an OPER dataset. Jewett (2007) has also applied MESO fields to derive realistic upper-tropospheric momentum fluxes for tropical convective cloud systems. MESO are also being provided to select U.S. National Weather Service offices across the upper Midwest to acquire feedback on their potential utility in an operational weather forecasting environment.

b. Validation of satellite-derived motions

It is important to note here that, like any other observing system, satellite-derived AMVs are inherently unable to perfectly depict the "true" flow at any given point and level in the atmosphere, even if optimal AMV target characteristics (horizontal dimension, cloud-top opacity/emissivity) and time behavior are present. The underlying assumptions of satellite-derived motion estimation are that features move 1) within a short-term image sequence at a constant height level, 2) without changing shape and acceleration, and 3) with speeds equal to the true atmospheric flow at a given level over the time interval of an image sequence. The first two assumptions can be violated in convective cloud scenes, especially if the image sequence separation time is large compared to the magnitude of vertical motions. The third assumption is difficult to evaluate with current generation observing systems as no "perfect" wind profiling instrument currently exists because of the presence of both instrument errors and small-scale atmospheric variability. In addition, vertical momentum transports occurring in "clear air" (i.e., cloud-free regions) induced by cumulus cloud dynamics and phenomena such as boundary layer eddies and gravity wave circulations cannot be directly measured from satellite. These transports can alter the actual flow measured by in situ rawinsonde or wind profilers. Studies have also shown that AMVs may better correspond to a layer of appreciable atmospheric depth rather than a single-level flow (Rao et al. 2002; Velden and Bedka 2009). The depth of this layer depends on environmental characteristics such as the vertical moisture distribution and wind shear, and the height, height assignment method, and type (satellite spectral channel, clear versus cloudy target) of AMV being considered.

Table 2 provides a brief summary of the target, time evolution behavior, and background wind analysis characteristics that would lead to an optimal AMV flow estimate using geostationary imagery. Because many of these guidelines cannot be fully satisfied with current generation operational satellite instrumentation, an appreciable portion of the AMV versus rawinsonde and profiler differences in this study could be related to deviations from these guidelines. It should also be noted that a combination of rawinsonde/profiler measurement errors, collocation matching–induced errors, and atmospheric temporal/spatial variability can contribute to

TABLE 2. A summary of target and background wind analysis characteristics that would lead to an optimal AMV using current generation geostationary AMV algorithms.

Optimal AMV target characteristics
Steady-state cloud features neither growing nor decaying in the vertical, with sharp, coherent edges
Cloud and WV targets represent a single/shallow tropospheric level/layer
A VIS or IR target should fill an entire 4-km IR pixel, with an opaque cloud top and an emissivity near 1, for the best application of the IR-based height assignment techniques
Targets for clear-sky WV tracking should represent a shallow layer of concentrated WV within the mid- to upper troposphere (Rao et al. 2002) and exhibiting sharp horizontal gradients
Distinct appearance of target's IR or VIS signature relative to the earth's surface (i.e., target much colder than surface, no surface snow or ice cover)
Targets within ~60° of the satellite nadir point; degradation can be expected outside of this radius toward the limbs of the satellite view
Optimal AMV target tracking and evolution behavior
Image temporal resolution: 5 min for VIS/IR and 30 min for WV (Velden et al. 2005)
Coherency in the shape and motion of the target over the tracking interval (low vertical shear environment; motion from advection, not acceleration)
Image-to-image georeferenced coregistration accuracy to within ~1 pixel
Optimal background analysis characteristics
For the applications discussed in this study, mesoscale NWP model analyses with high spatial and vertical resolution to obtain accurate, representative temperature profiles for use in AMV height assignment

AMV and rawinsonde/profiler comparison differences to be shown later.

3. Applications of mesoscale AMVs to weather diagnosis and forecasting

Before AMV validation statistics are presented, we will first discuss the application of MESO to weather diagnosis and forecasting. This section focuses on two events over the central United States, the first occurring on 13 June 2005 with complex flow patterns associated with a midlatitude cyclone, and the second occurring on 8 June 2005 with mesoscale confluence and convective storm initiation.

a. Case event 1: 13 June 2005

For the 13 June event, Fig. 1 illustrates the cloud field associated with a weather system as observed by the GOES-12 1-km VIS channel at 1645 UTC. A well-defined cyclonic circulation is centered along the Nebraska–South Dakota border, fair-weather cumulus are to the southeast in the warm sector, and a surface convergence zone (shown in blue) defines the boundary between a very warm, moist air mass present in the southeast United States and drier air to the northwest. This boundary served as the focus for severe thunderstorm development later in the day (see Fig. 2).

Figure 3 shows the AMV fields depicted using both the OPER and MESO methods corresponding to the imagery shown in Fig. 1. For this particular image sequence, 6239 vectors were identified using the MESO method, as compared with 1108 conventional OPER

winds. Although the primary features of this scene, the cyclonic circulation and southerly flow within the warm sector, are captured by both AMV types, subtle differences exist that have important implications for weather diagnosis and forecasting for this case.

We first focus on mid- to upper-level flow associated with a well-defined cyclonic circulation over the central Great Plains. Analysis of animated multispectral satellite imagery by a human expert positioned the cyclonic circulation over north-central Nebraska at the red X in Figs. 4a and 4c. This is depicted very well by the MESO field (Fig. 4c), but much less so by OPER (Fig. 4d), which portrays a much broader, elongated circulation extending across northern Nebraska and eastern South Dakota. Figure 4b shows that the NOGAPS 6-h forecast wind field, used as a first guess within the OPER method, also positions the cyclonic circulation farther to the east of that shown by MESO. The difference in positions can be attributed in part to the ~1-h time difference between the NWP and AMV fields. As this circulation is depicted fairly well by the first guess, the results suggest that the spatial targeting sizes used for OPER IR and WV were too large to capture this feature (15 × 15 ~4-km-resolution pixels = ~720 km^2 at subsatellite point, but larger over this central U.S. domain). In contrast, the smaller targets (5 × 5 pixels = ~25 km^2 for ~1-km VIS and ~400 km^2 for ~4-km IR and WV) tracked in the upper troposphere allowed MESO to resolve the mesoscale circulation. The MESO field also captured a region of higher wind speeds (≥25 m s^{-1}) across western Minnesota and the eastern Dakotas, which is represented in the Navy Operational

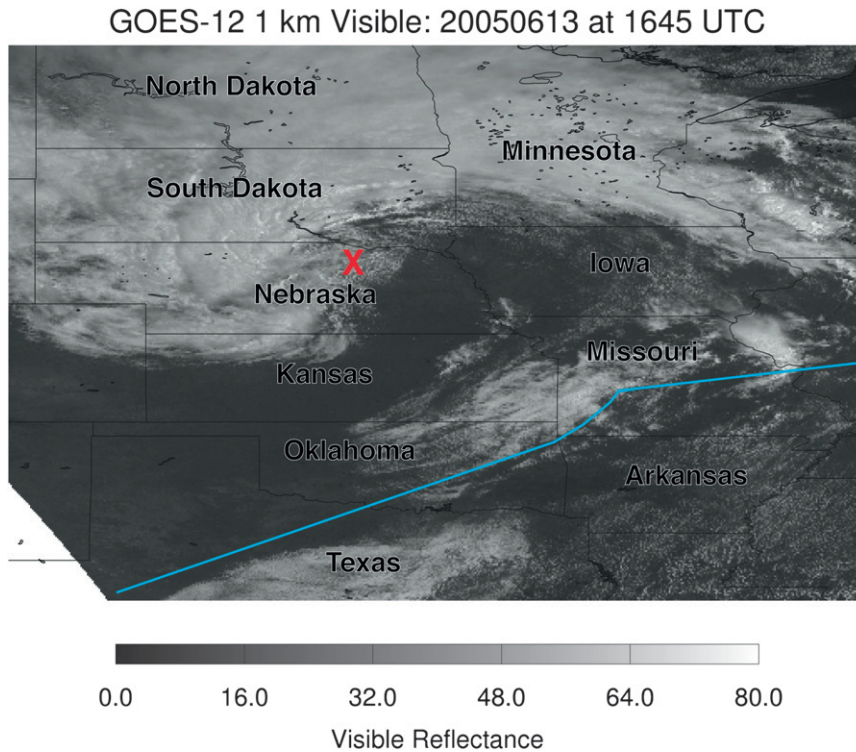## GOES-12 1 km Visible: 20050613 at 1645 UTC

FIG. 1. *GOES-12* 1-km VIS imagery at 1645 UTC 13 Jun 2005. The location of a surface convergence line, as identified by a human analyst using surface observations from 1700 UTC, is highlighted in blue, which separates a warm, humid air mass to the south from drier air north and west of the boundary. The red X illustrates the circulation center of a midlatitude cyclone.

Global Atmospheric Prediction System (NOGAPS) field but absent from OPER. These factors further highlight the benefits of detailed feature tracking in detecting subtle regions of enhanced upper-level jet flow.

Low-level flow within the warm sector of this system from MESO, OPER, and NOGAPS is shown in Fig. 5. A surface boundary served as the focus for severe thunderstorm development from 1900 to 2100 UTC. To the southeast of the boundary, southerly winds of $\sim$5 m s^{-1} are represented by both AMV types across eastern Texas, Louisiana, and Mississippi, a bit slower than those from the NOGAPS.

Higher speed flow is found across northern Arkansas and southern Missouri for both AMV types and NOGAPS. MESO, however, detects a narrow corridor of higher wind speed and variability (outlined in black) not present in OPER, with several vectors exceeding 20 m s^{-1}. The NOGAPS forecast shows a region of enhanced speed across southern Arkansas, but does not extend this speed maximum to the southwest as depicted by MESO. The location of this narrow low-level jet is highly correlated with thunderstorms that produced severe winds, whereas storms to the southwest in a weaker flow were primarily hail producers (see Fig. 2).

Several tornado reports were in this higher–wind speed region, indicating that the MESO product may have depicted a localized region of enhanced low-level wind shear favorable for tornadogenesis.

Another significant difference between MESO and OPER is found along and to the north of the surface boundary in Oklahoma. MESO depicts low-level flow from the NW with numerous vectors. This flow is not present in either OPER or the NOGAPS forecast. These MESO vectors were obtained from the fine northwest–southeast-oriented cumulus cloud streets in central Oklahoma. Studies have indicated that the cloud-top flow is generally within 10°–20° of the orientation of cloud streets (Lemone 1973). The Lamont NOAA wind profiler (not shown) further validates the presence of northwesterly flow in this region at this time. The cloud streets and northwesterly MESO flow extend to the south of the surface boundary, suggesting some tilting with height.

b. Case event 2: 8 June 2005

Figure 6a shows *GOES-12* VIS imagery at 1702 UTC with small cumulus present across northeast Kansas, a
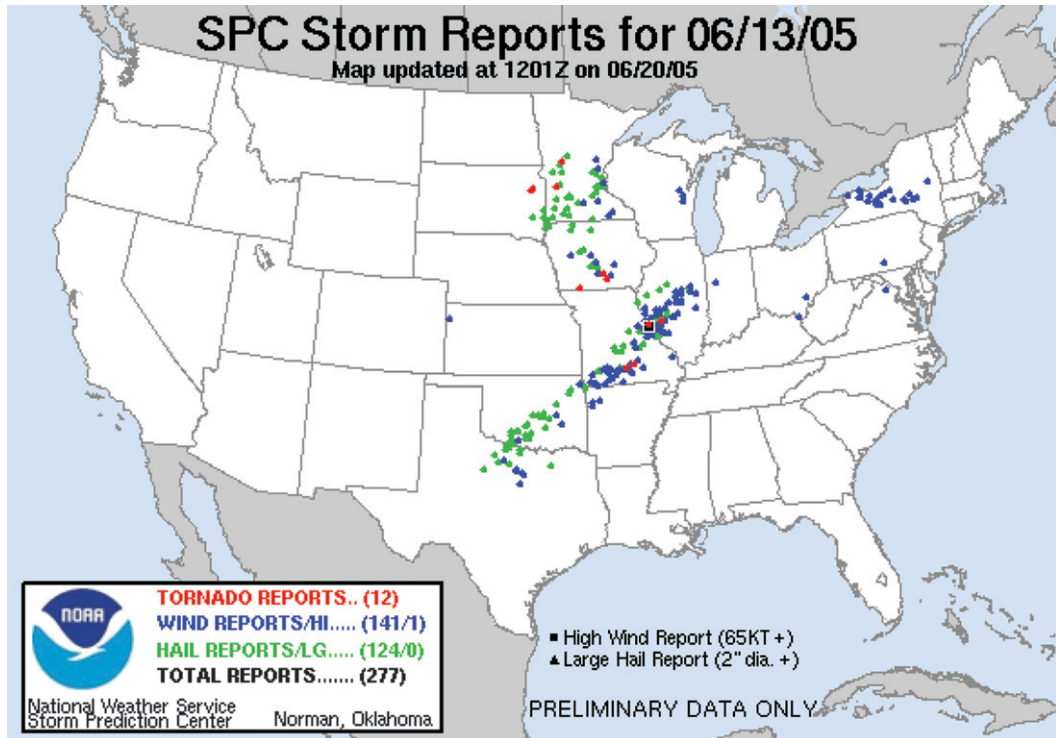
FIG. 2. Severe thunderstorm reports from 1200 UTC 13 Jun to 1159 UTC 14 Jun 2005. Reports present along and north of the surface boundary shown in Fig. 1 occurred after 1930 UTC, nearly 3 h after the period of focus for this paper.
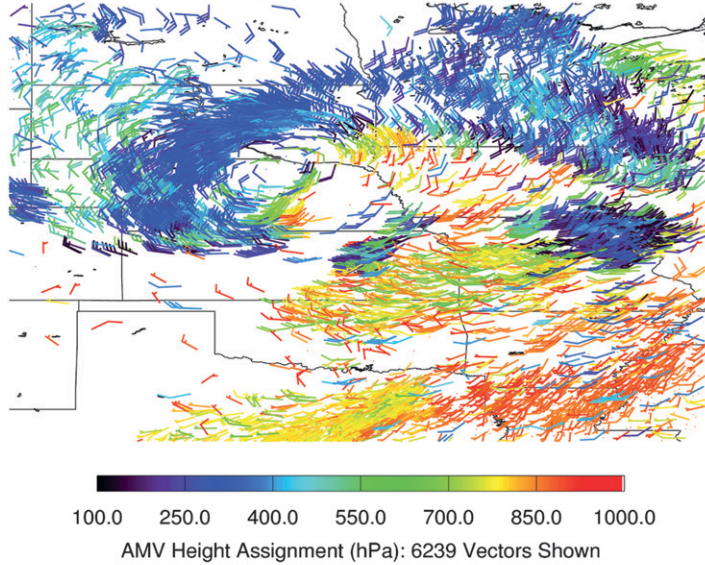
large convective storm complex in northern Missouri and southern Iowa, and convective outflow and a cloud band trailing to the west-southwest of this complex. The movement of this cloud band from 1602–1732 UTC (as identified by a human analyst) illustrates the progression of the band in VIS imagery to the east-southeast over this time window. By 2332 UTC (Fig. 6b), the region of small cumulus in central Kansas has developed into a line of deep convective storms, indicating that sufficient forcing was present at earlier times to initiate convection.

The MESO field in Fig. 7a is annotated to show the locations of features described within 1702 UTC VIS imagery. MESO shows confluence occurring at this time in association with the small cumulus field in central Kansas and that the two areas of outflow were propagating southward away from the convective complex. Although the multiple MESO observations show a systematic turning of the wind along the entire confluence zone, the only indication of confluence in the OPER field at this time is one wind barb to the southwest. Within the 1700 UTC wind profiler and 1800 UTC rawinsonde observations (see Fig. 7c), the horizontal scale of the confluence was much larger. The confluence is occurring over a spatial scale that is not well resolved by OPER processing and in a region with a relatively high number, but still inadequately spaced, upper-air observations. MESO processing clearly resolves this flow pattern, which likely contributed to forcing deep convection in the following hours.

MESO also captures the southeastward movement of the cloud band in southeast Kansas, though with some spatial variability in the vector field. In contrast, OPER shows only two westerly wind barbs with a higher height assignment than vectors depicted by MESO (~700 hPa for OPER, ~800 hPa for MESO). The IR window brightness temperature T_B of this band was ~288 K, which corresponds to a pressure height of ~785 hPa and agrees better with the MESO height assignment when compared to the nearby Lamont 1800 UTC sounding (not shown). The Neodesha, Kansas, profiler (black box, Fig. 7c) indicates southwesterly flow at 850 hPa, even though this profiler is perfectly situated to observe the motion and passage of the cloud band. A time–height display of Neodesha profiler observations (see Fig. 8) shows that northwest winds are not observed at any time between 1630 and 1730 UTC and below the 500-hPa level. The flow from 500–200 hPa (not shown) becomes southwesterly and would not likely have an impact in moving this low cloud band. As a human analyst can clearly identify the southeastward

GOES-12 Mesoscale Atmospheric Motion Vectors: 20050613 at 1645 UTC

100.0   250.0   400.0   550.0   700.0   850.0   1000.0

AMV Height Assignment (hPa): 6239 Vectors Shown

GOES-12 Operational Atmospheric Motion Vectors: 20050613 at 1645 UTC

100.0   250.0   400.0   550.0   700.0   850.0   1000.0

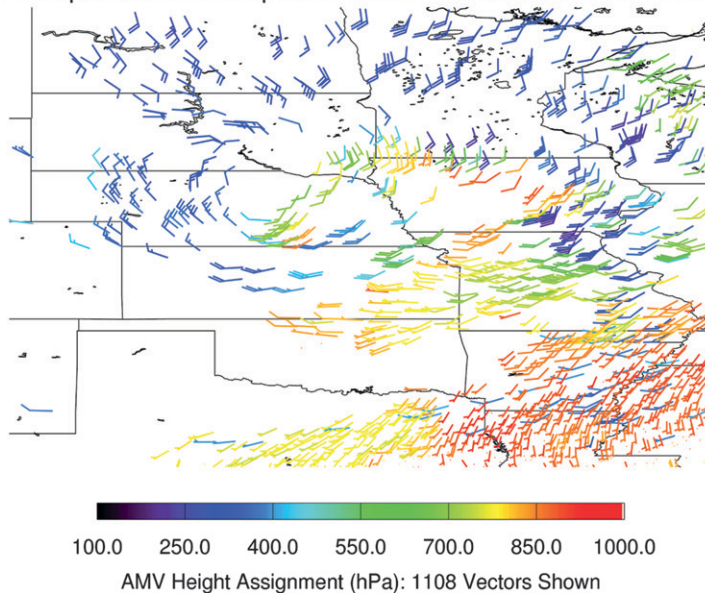AMV Height Assignment (hPa): 1108 Vectors Shown

FIG. 3. (top) MESO over the central United States at 1645 UTC 13 Jun 2005. Vectors are colored by AMV height assignment. (bottom) OPER acquired using the same three-image sequence. A full (half) wind barb represents a wind speed of 10 m s^{-1} (5 m s^{-1}).

motion of this band and the satellite-derived AMVs attempt to represent what a human observes through the objective tracking of cloud gradient patterns, this calls into question the fundamental assumption of AMV algorithms and validation studies in that 1) clouds are nondeveloping features that are transported by the surrounding flow and 2) the satellite-observed cloud motions should match the actual wind flow at a single atmospheric level.

4. Validation data and methodology

For the statistical validation component of this study, *GOES-12* experimental MESO and NOAA/NESDIS OPER AMVs within 25 km of the Lamont 404-MHz NOAA wind profiler site (LMNO2) were collected over a 1-yr period from April 2005 to 2006, providing a database of 15 332 MESO and 1132 OPER VIS, WV, and IR window channel vectors. MESO AMVs are processed
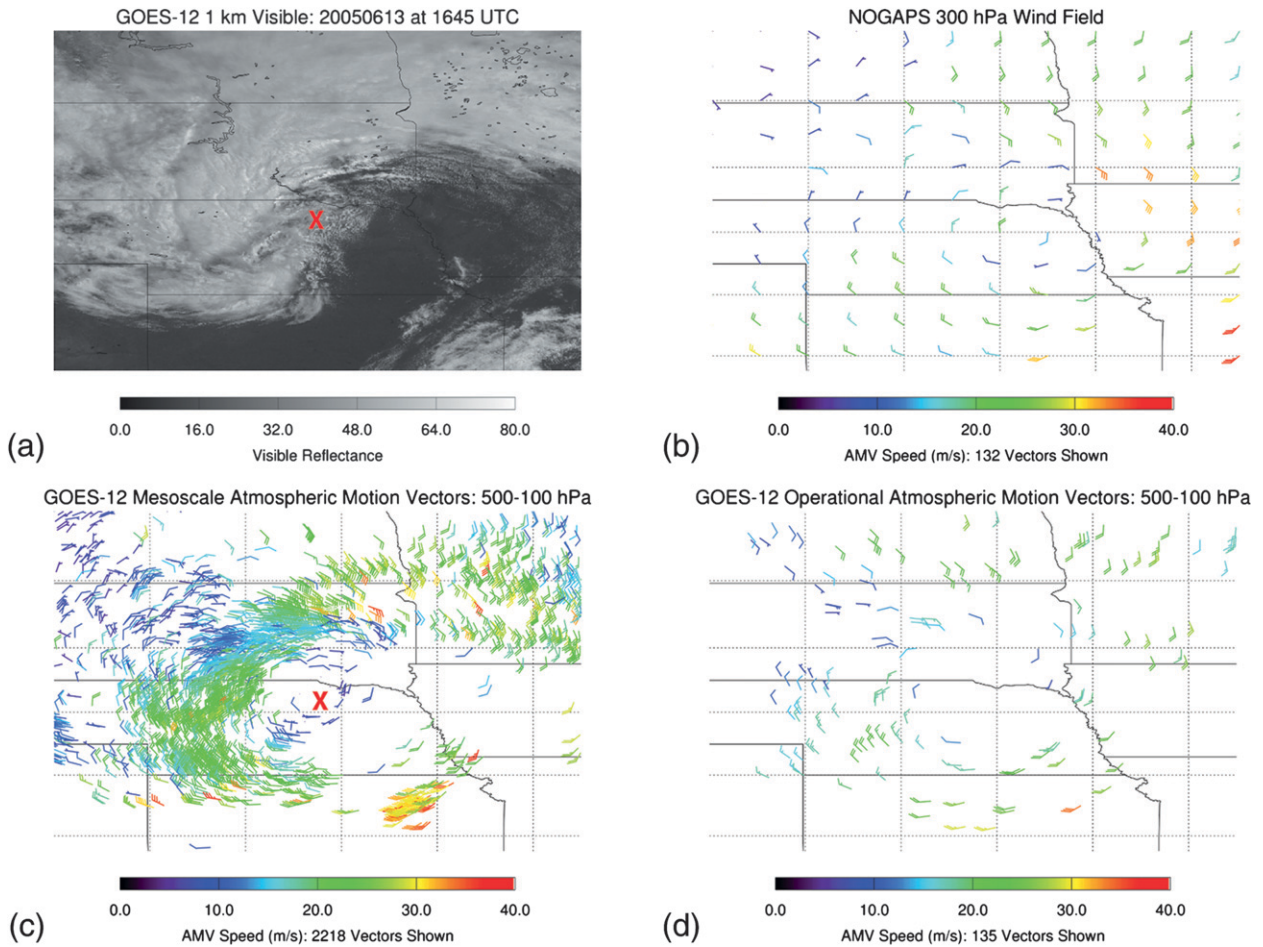
FIG. 4. (a) *GOES-12* 1-km VIS channel imagery centered on a closed low pressure center over the U.S. central Great Plains at 1645 UTC. (b) NOGAPS model 6-h forecast of the 300-hPa wind field valid at 1800 UTC. (c) All MESO within the 500–100-hPa layer at 1645 UTC. (d) All OPER within the 500–100-hPa layer at 1645 UTC. Wind barbs are colored by wind speed (m s^{-1}). A full (half) wind barb represents a wind speed of 10 m s^{-1} (5 m s^{-1}). The red X illustrates the center of circulation of the cloud field as identified by a human analyst.

every 15–30 mins during the daytime in support of convective storm nowcasting applications, which require use of the GOES VIS channel. The MESO processing scheme is by no means limited to daytime operations, but a high percentage of the AMV information is provided through VIS channel cloud tracking. OPER AMVs are processed during both day and night every 3 h in support of global NWP model assimilation and other NOAA operations. Both OPER and MESO datasets use a minimum wind speed of 4 m s^{-1} to mitigate depiction of spurious motions that could be caused by errors in satellite data navigation and/or image-to-image registration.

Three sets of comparisons will be shown in the following section. One comparison incorporates collocated AMV, wind profiler, and rawinsonde observations. These results are shown to evaluate MESO accuracy versus the rawinsonde, which is generally used within

the literature to evaluate the quality of satellite AMV products (see Nieman et al. 1997; Velden et al. 2005). The results from this comparison will also demonstrate the relative accuracy and consistency of 404-MHz wind profiler observations, as few AMV validation studies have been performed with this data (Susko and Herman 1995). The statistics used in the comparison of these datasets are vector root-mean-squared difference (VRMS), directional RMS (DRMS) and wind speed bias. The equations used to compute these statistics are described by Nieman et al. (1997).

Once proof of profiler measurement consistency and accuracy has been established, a second set of comparisons focuses exclusively on AMV and profiler data matches, which provide a much larger sample size of collocated wind observations. This will allow for match statistics to be separated by AMV height and quality-control parameter
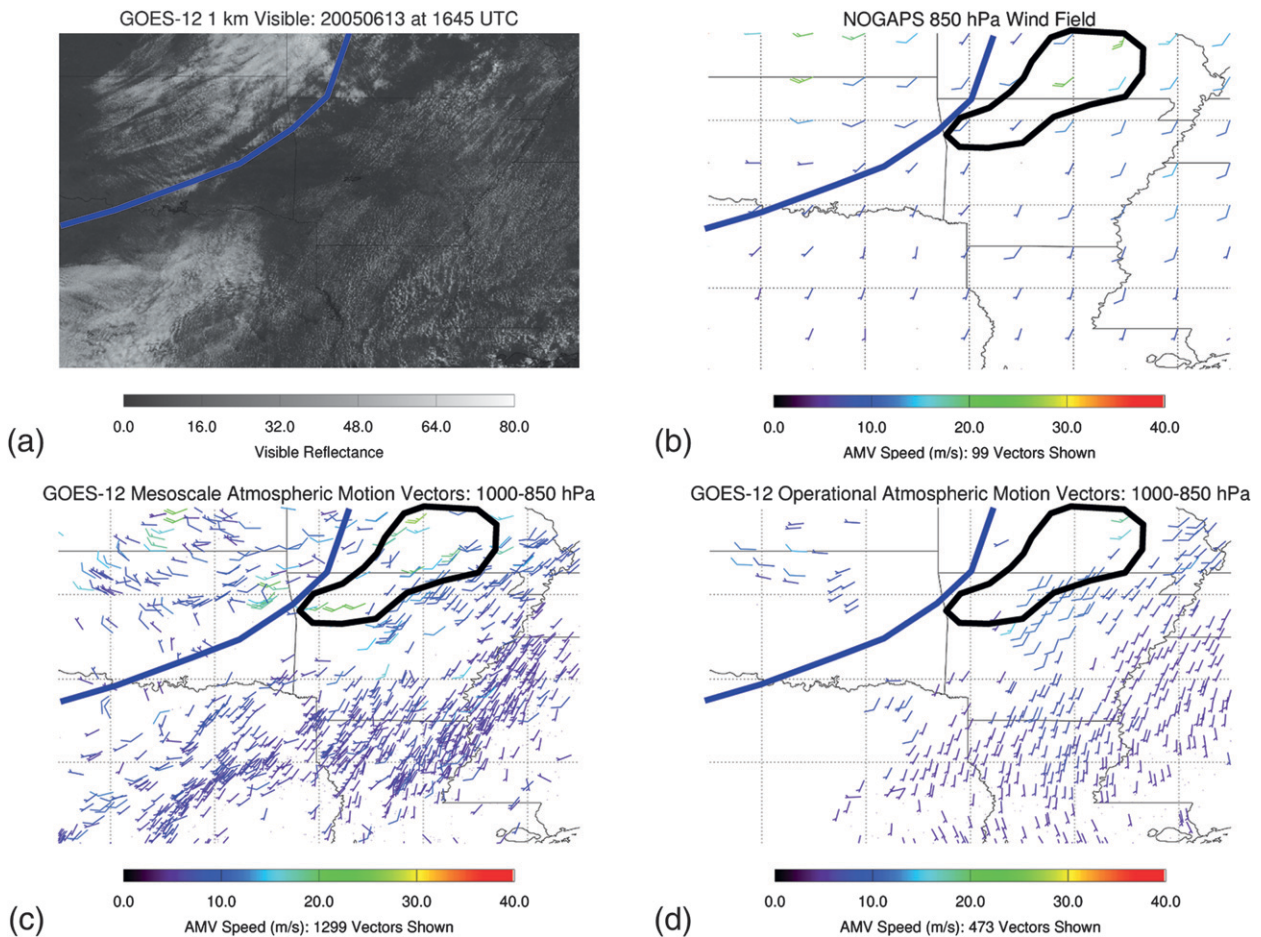
FIG. 5. (a) *GOES-12* 1-km VIS channel imagery centered on an airmass boundary over the Southern Great Plains at 1645 UTC. (b) NOGAPS model 6-h forecast of the 850-hPa wind field valid at 1800 UTC. (c) All MESO within the 1000–850-hPa layer at 1645 UTC. (d) All OPER within the 1000–850-hPa layer at 1645 UTC. Wind barbs are colored by wind speed (m s^{-1}). A full (half) wind barb represents a wind speed of 10 m s^{-1} (5 m s^{-1}). The blue line represents the approximate location of a surface boundary, as identified by a human analyst using surface observations from 1700 UTC. The black line outlines a narrow low-level jet identified within the MESO field.

information. Last, a direct comparison between MESO and OPER will be shown for situations where the two methods found an AMV from near-identical scenes. Table 3 provides a summary of the spatial and temporal match criteria for these comparisons.

Vaisala RS-92 rawinsonde wind profiles are compared to AMVs and 6-min wind profiler observations to evaluate the relative accuracy of these wind estimates versus an accepted standard for wind measurement. Four rawinsondes are launched per day in normal operations at the SGP Central Facility. When supplemental rawinsondes from intensive observation periods are added to the operational rawinsonde database, quality-controlled data from 1628 rawinsondes are included in this study. The measurement accuracy of the Vaisala RS-92 rawinsondes, which use a Loran C windfinding system near the ARM SGP site, is esti-

mated to be 0.5 m s^{-1} (Coulter et al. 2005). For reference, the rawinsonde launch site is located 7 km away from the Lamont 404-MHz wind profiler site.

Quality-controlled 6-min resolution data from the Lamont 404-MHz NOAA wind profiler are compared to GOES AMVs to evaluate AMV speed and direction. Since satellite AMVs are height assigned to pressure levels, the profiler sampling levels must be converted from altitude (in meters) to pressure (in hPa) to directly compare the two datasets. This conversion is performed using a time-matched initial analysis pressure/height profile from the operational Rapid Update Cycle 20-km resolution model run (RUC-20; Benjamin et al. 2002) for the model grid point closest to the ARM site. As a three-image sequence of 15-min resolution *GOES-12* data is most often used to compute AMVs, at least five of the six possible 6-min wind profiles within this 30-min
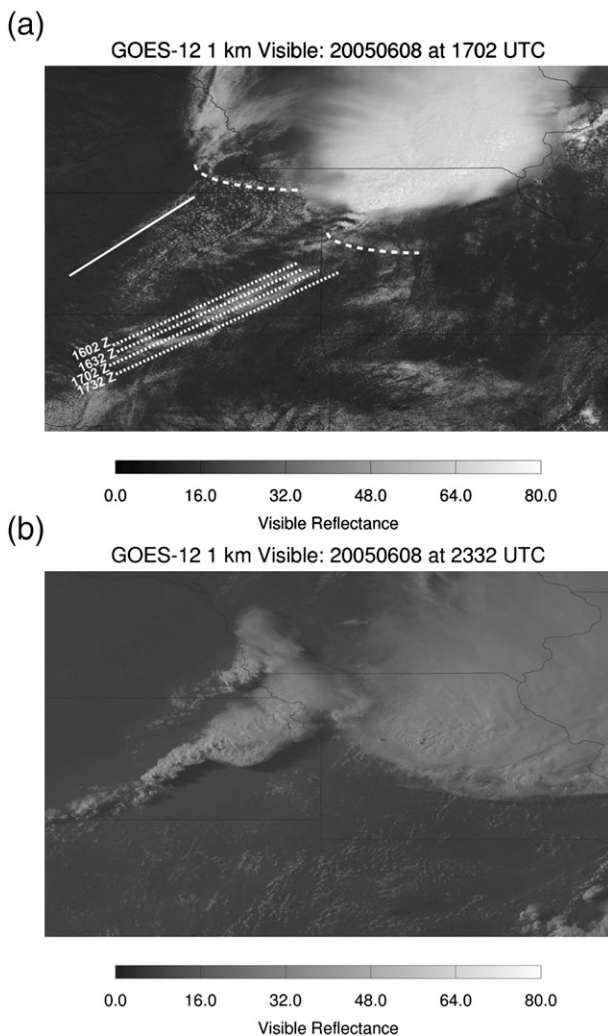
(a)

GOES-12 1 km Visible: 20050608 at 1702 UTC

(b)

GOES-12 1 km Visible: 20050608 at 2332 UTC

FIG. 6. *GOES-12* 1-km VIS imagery at (a) 1702 UTC and (b) 2332 UTC 8 Jun 2005. The location of a line of small cumulus is identified with a solid line and two convective outflow boundaries are identified with a dashed line in (a). The location and extent of a cloud band at 1602, 1632, 1702, and 1732 UTC in southeast Kansas and northern Oklahoma is shown with a dotted line in (a).

window are time averaged together (centered in time on the middle GOES image) to remove small-scale wind variability and provide a set of wind observations that is reasonable and "fair" to compare with GOES AMVs. Vectors above the 7500-m level are matched only with profiler "high mode" observations, as a much greater number of high-mode observations pass quality-control checks than those from the low mode within the profiler "overlap region" extending between 7500 and 9250 m (Petersen and Bedka 2007).

It is understood that neither rawinsondes nor wind profilers provide absolute truth wind measurements, but merely offer stable, well-calibrated comparison

datasets. The wind profilers have the advantage of providing high–temporal resolution observations, which allow for a large sample database of well-collocated AMV and profiler observations. In contrast, wind observations from rawinsonde may be slightly more accurate, but the limited number of observations made during normal SGP Central Facility operations greatly reduces the possible data matches. Detailed comparisons of ~400-MHz UHF wind profiler and rawinsonde wind observations through the full depth of the troposphere are shown by Weber et al. (1990) for the hourly operational profiler product and Petersen and Bedka (2007) for the 6-min-resolution product. Validation of a half-hourly averaged wind profiler product using ground-based radar wind estimates is described by Yoe et al. (1992).

5. Results of AMV quantitative assessment

a. Comparison of MESO and NOAA wind profiler to rawinsonde

Figure 9 provides a set of scatter diagrams for the 2272 collocated MESO, wind profiler, and rawinsonde observations. These results are shown to evaluate MESO accuracy versus the rawinsonde, which is generally regarded as the standard for accuracy in wind measurement, as well as to validate 404-MHz 30-min mean wind profiler observations. Very close agreement exists between rawinsonde and profiler observations, with a VRMS of 2.92 m s^{-1}, DRMS of 14.3° (not shown), and near-zero speed bias. Wind component differences show a limited degree of scatter but no data points have a component difference larger than 10 m s^{-1}. Close agreement between wind profiler and rawinsonde observations contributes to similar VRMS for both the AMV–profiler (8.5 m s^{-1}) and AMV–rawinsonde (8.7 m s^{-1}) comparisons. Wind speed and vector biases are nearly identical as well.

Although the previous analysis generally indicates close agreement between rawinsonde and profiler, it is also important to examine the relative accuracy of profiler data with height. Figure 10 provides a comparison between profiler and rawinsonde wind data where the rawinsonde was within 0–25 km of the profiler site, the same distance criteria that will be used for AMV–profiler comparisons. This comparison shows that VRMS differences between 2 and 3 m s^{-1} are present within the 700–200-hPa pressure layer and there is a significant VRMS increase above and below this layer. The larger low-level differences are likely the result of increased local variability due to mixing processes within and at the top of the boundary layer. The larger

GOES-12 Mesoscale Atmospheric Motion Vectors: 20050608 at 1702 UTC

GOES-12 Operational Atmospheric Motion Vectors: 20050608 at 1702 UTC

(a)

100.0   250.0   400.0   550.0   700.0   850.0   1000.0
AMV Height Assignment (hPa): 770 Vectors Shown

(b)

100.0   250.0   400.0   550.0   700.0   850.0   1000.0
AMV Height Assignment (hPa): 159 Vectors Shown

NOAA Operational 850 hPa Observations: 20050608 at 1700 and 1800 UTC
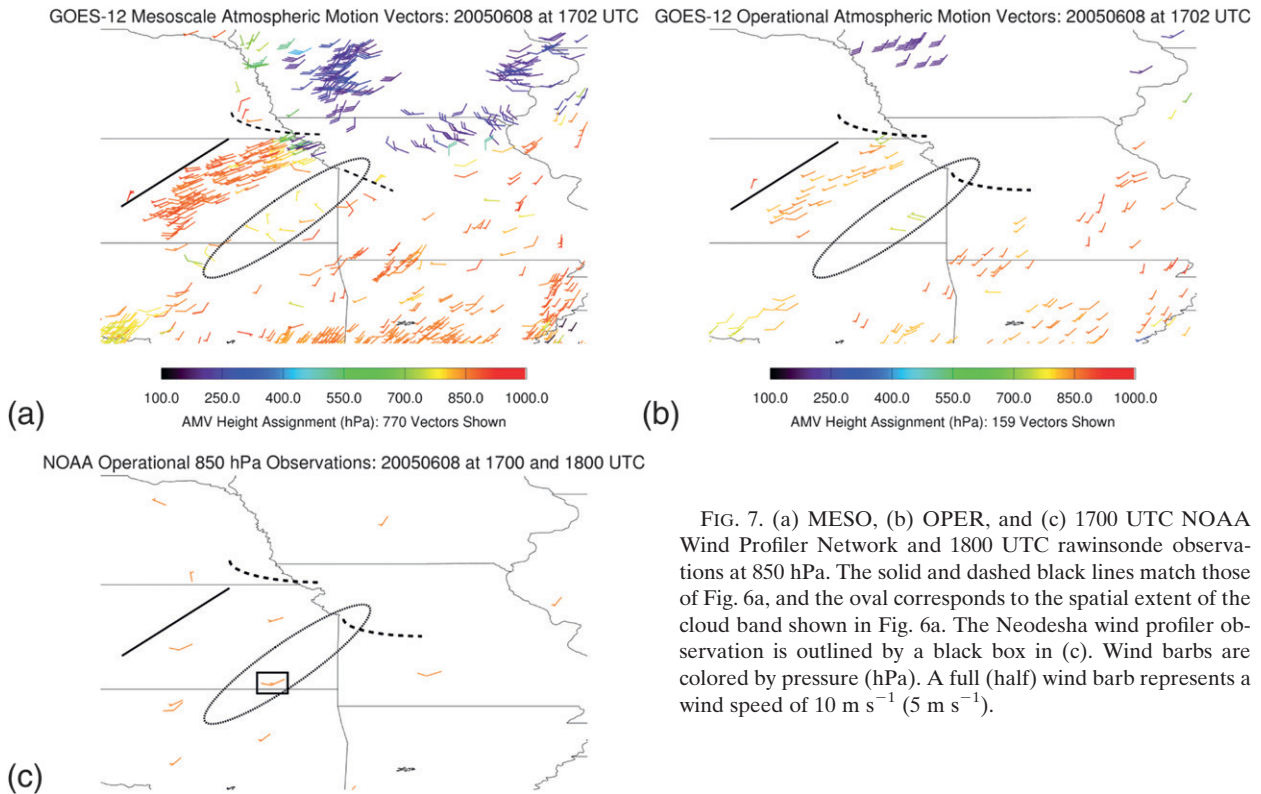
(c)

FIG. 7. (a) MESO, (b) OPER, and (c) 1700 UTC NOAA Wind Profiler Network and 1800 UTC rawinsonde observations at 850 hPa. The solid and dashed black lines match those of Fig. 6a, and the oval corresponds to the spatial extent of the cloud band shown in Fig. 6a. The Neodesha wind profiler observation is outlined by a black box in (c). Wind barbs are colored by pressure (hPa). A full (half) wind barb represents a wind speed of 10 m s^{-1} (5 m s^{-1}).

differences aloft can be attributed to both increased profiler instrument error and the fact that the decreased vertical resolution of high-mode profiler data may not be able to fully capture the strong vertical wind shear that often occurs near the tropopause.

A full description of this comparison and an analysis of spatial and temporal wind variability is provided by Petersen and Bedka (2007). The results of the Petersen and Bedka study and those of Figs. 9 and 10 demonstrate that good confidence can be placed in quality-controlled 6-min NOAA Wind Profiler Network data within the 700–200-hPa layer. Though we will compare AMVs to profiler observations within the entire 1000–100-hPa layer in the following section, care must be taken in interpreting the results above 200 hPa.

b. Comparison of NOAA wind profiler to MESO and OPER

A comparison between MESO and NOAA wind profiler observations is shown in Fig. 11. For the 11 832 comparisons shown here, the VRMS (DRMS) is 8.5 m s^{-1} (34°). Bias statistics reveal that the mean MESO speed is 0.48 m s^{-1} faster than the mean profiler speed, with the mean direction differing by only 1.7°. Scatter point maxima (in grayscale) are found along the diagonal in

Figs. 11a and 11b and near the origin in Fig. 11c. Points found in the upper left and lower right of Fig. 11c are a function of the fact that wind direction varies from 0° to 360°, and they do not necessarily represent large differences in direction or adversely affect the statistical comparisons between MESO and profiler [e.g., a direction observation of 359° is very close to a 1° observation; see Fisher (1993) for a description of directional comparison methodology]. MESO provides "good" wind estimates for 43% of the total vector matches (5087 out of 11 832 vectors), if good is defined as a vector difference of less than 5 m s^{-1} (not shown). Figure 12 (black bars) shows that MESO matches are well distributed throughout the troposphere, with a slight maximum in the 150–300-hPa pressure layer.

Figure 13 is similar to Fig. 11 except that OPER produced by NOAA/NESDIS are compared with profiler data. For the 721 comparisons shown here, the VRMS (DRMS) is 5.6 m s^{-1} (18°). These statistics show that significantly better agreement exists between the coarser-resolution OPER and profiler wind observations than that from the larger number of higher-resolution MESO comparisons described above. Tighter clustering along the diagonal can be seen in Figs. 13a,b, and the origin in Fig. 13c, with fewer outliers than the MESO comparisons relative to the total number of matches.
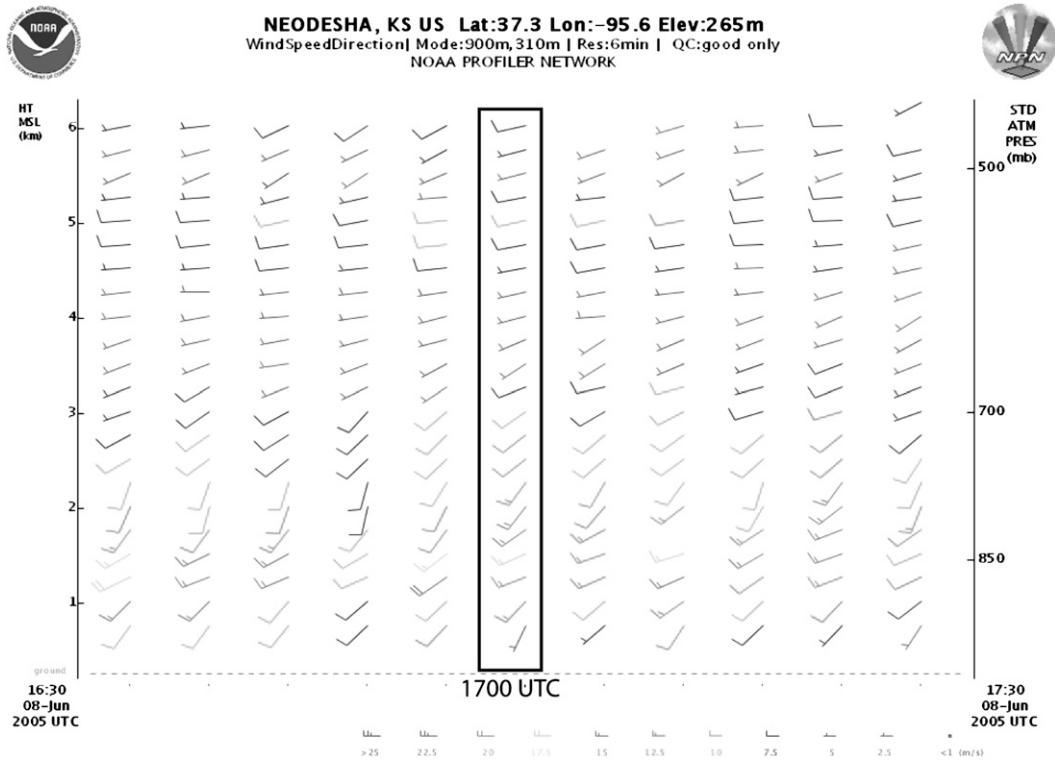
FIG. 8. A time–height display of 6-min wind profiler observations from the Neodesha profiler site between 1630 and 1730 UTC 8 Jun 2005. The 1700 UTC wind profile is outlined by a black rectangle, which corresponds to the time of the wind fields depicted by MESO and OPER in Fig. 7. A full (half) wind barb represents a wind speed of 10 m s^{-1} (5 m s^{-1}).

The mean wind speed observed by OPER AMVs is ~3.6 m s^{-1} faster than MESO. This may be related to the fact that ~81% of the data matches are found within the 400–100-hPa layer (see Fig. 12, exact percentage between 400 and 100 hPa not explicitly shown), which corresponds well with the height range of the tropospheric wind speed maximum over the central United States. Based upon the above definition, OPER exhibits good agreement with the profiler for 65% (469 out of 721 vectors) of the data matches.

As MESO–profiler differences are significantly larger than those of OPER, we will examine the scene characteristics for significant outliers in Fig. 13 to better understand scenarios for which MESO and profiler exhibit poor agreement. For this analysis, we consider a significant outlier as a MESO–profiler vector difference greater than three standard deviations from the mean vector difference. The mean (standard deviation) vector difference of 11 832 MESO–profiler matches was 6.85 m s^{-1} (5.04 m s^{-1}). We are examining matches with a vector difference greater than ~22 m s^{-1}, which provides 141 vectors for this analysis. *GOES-12* animated multispectral imagery is examined for these vectors and three primary scene types were associated with 97% of

the outlier AMVs. The three scene types were those featuring cirrus (53% of outliers), multilayered (33%), and cumuliform (both immature and deep convective; 11%) clouds. Thin cirrus and multilayered clouds represent a significant challenge for IR-based cloud-top and AMV height assignment algorithms, so the fact that these situations represent the vast majority of the outliers is expected. As shown by the 8 June 2005 case in section 3, the apparent motion of cumuliform clouds in satellite imagery can differ significantly from the observed wind flow, contributing significant ''error'' to the comparison statistics.

Additional statistics for matches separated by pressure-level and quality-control parameter information are provided to further characterize and understand the AMV–profiler differences described above (Tables 5, 6). Table 4 provides a summary of the aforementioned statistics for the entire match database and will serve as a reference for the discussion below.

The results in Table 5 can be used to better understand the relative accuracy of AMVs with height. MESO AMVs within the lowest layer (1000–851 hPa) exhibit the highest DRMS, as well as a slightly negative speed bias relative to other layers. The limited number of

TABLE 3. A summary of dataset match criteria for MESO, OPER, wind profiler, and rawinsonde statistical comparisons.

Datasets compared	No. of matches	Horizontal match criterion	Vertical match criterion	Temporal match criterion
Comparison 1: Collocated NOAA wind profiler, rawinsonde, and MESO				
NOAA wind profiler and rawinsonde	2272	25 km	2 hPa	±3 min
NOAA wind profiler and MESO	2272	25 km	10 hPa	30-min mean profiler data centered on AMV time
Rawinsonde and MESO	2272	25 km	2 hPa	Balloon launch within ±30 min of MESO time
Comparison 2: Collocated NOAA wind profiler with MESO and OPER				
NOAA wind profiler and MESO	11 832	25 km	10 hPa	30-min mean profiler data centered on AMV time
NOAA wind profiler and OPER	721	25 km	10 hPa	30-min mean profiler data centered on AMV time
Comparison 3: Direct comparison between MESO and OPER				
MESO and OPER	247	50 km	25 hPa	30 min

OPER–profiler matches from the 1000–701-hPa layer exhibit relatively high DRMS as well. For 271 MESO–rawinsonde matches below the 850-hPa level, comparison with rawinsonde data shows a VRMS (DRMS) of 6.94 m s^{-1} (42.3°) (not shown), significantly lower than the results for profiler comparisons shown in Table 5. When 386 MESO–rawinsonde matches are evaluated within the 850–701-hPa layer, the results are much closer to those shown in Table 5, with a VRMS (DRMS) 8.17 m s^{-1} (37.2°). AMV–rawinsonde differences from the mid- and upper layers also agree very well with those from the AMV–profiler comparisons (not shown). Because it is possible though that unrepresentative wind measurements were collected by rawinsonde between 1000 and 850 hPa, the true wind may lie somewhere in the middle of the observations collected by the two instruments. However, the profiler–rawinsonde comparison from Fig. 9 suggests that it is more likely that a portion of the increased low-level AMV–profiler differences arises from comparisons in situations with significant spatial wind variability or local boundary layer mixing.

The purpose of AMV quality-control algorithms such as QI is to objectively determine the relative accuracy of an AMV. Holmlund (1998) describes the following five tests that are used to formulate the QI score parameter, subvector 1) speed, 2) vector, and 3) directional differences, 4) spatial consistency with neighboring AMVs, and 5) NWP model forecast agreement. Thus, an OPER with a high-QI parameter value represents consistent satellite-derived flow across a three-image sequence and good agreement with neighboring AMVs and an interpolated NWP model (NOGAPS) forecast wind vector. The effect of test 5 is removed from MESO processing to minimize the NWP model influence on the resulting vector field.

An evaluation of the impact of changing algorithm quality-control parameters on relative AMV accuracy is shown in Table 6. For QI, a score of 1 would be considered the most accurate possible depiction of the atmospheric flow at the specified level, with lower scores indicating a lesser accuracy. While the QI algorithm was developed using vectors from OPER processing settings, the comparisons here will study whether or not QI information can be used to identify MESO of higher relative accuracy. It should be noted here that because QI score data were not available for both May and September 2005, the table only includes 506 out of the 721 total OPER data matches. The results show that AMVs with higher QI parameter values exhibit better agreement with profiler data. OPER AMVs with high QI scores compare exceptionally well, with vector and directional RMS differences of and 4.6 m s^{-1} and 9.2°. For the lowest QI score range, OPER AMV RMS differences are much higher than those from the entire match database. MESO AMV–profiler vector differences are reduced by 1.5 m s^{-1} (17%) when the QI score increases from the lowest to the highest range.

Table 7 provides a summary of the MESO–profiler agreement after removal of all MESO derived from the thin cirrus and deep convection scene types and the application of stringent QI-based quality control. Multispectral imagery from the entire 1-yr MESO database was examined to identify vectors from these two "outlier" scene types. All MESO from multilayered clouds could not be definitively identified for the entire database, so these remain in the AMV database with the understanding that the AMV–profiler agreement would likely improve even further if they could be effectively removed. As implied in the outlier analysis above,
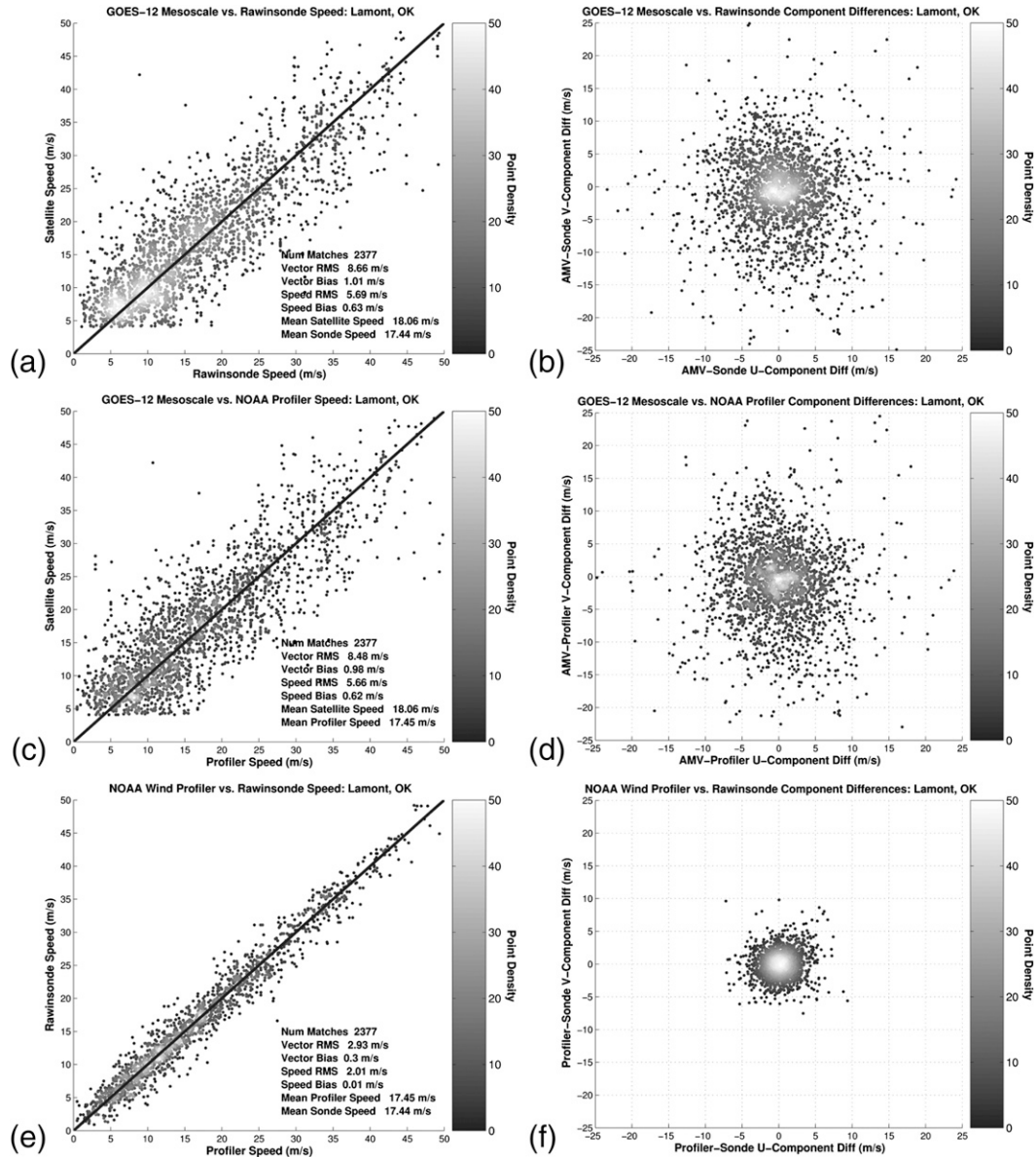
FIG. 9. (a) A comparison of MESO speed (m s^{-1}) with rawinsonde wind observations for the 1-yr study period. Positive speed biases indicate that MESO wind speeds are faster than profiler/rawinsonde observations. (b) MESO vs rawinsonde u- and v-component wind differences. (c),(d) As in (a),(b) but MESO and NOAA wind profiler observations are compared. (e),(f) As in (a),(b) but NOAA wind profiler and rawinsonde observations are compared. Positive speed biases in (e) indicate that profiler wind speeds are faster than rawinsonde observations. All validation statistics in plot legends are also in meters per second.

Table 7 shows that MESO–profiler VRMS is higher than the total match database VRMS for AMVs from these two scene types. Poor agreement for deep convection cases does not necessarily imply that MESO were grossly incorrect, since deep convection can induce significant spatial wind variability within the 0–25-km match radius. AMVs from these two types represent ∼20% of the total database (2412 of 11 832 total MESO)

and their removal improves the AMV–profiler match agreement by 0.20 m s^{-1} over the total VRMS shown in Table 4. A "best case scenario" is also presented in Table 7, where the outlier AMV types are removed in addition to the QI score being increased to a value at or above 0.90. VRMS agreement for this scenario is 1.81 m s^{-1} higher than that of the total OPER database with nearly 3 times the number of vectors.
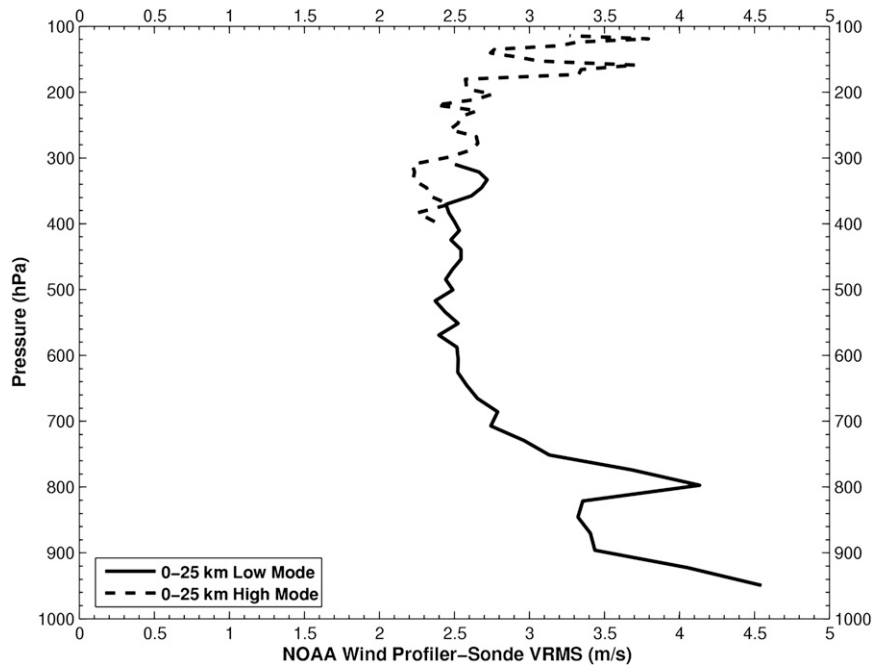
FIG. 10. The VRMS difference between Lamont 6-min wind profiler and rawinsonde observations from April 2005 to 2006 when the rawinsonde was within 25 km of the profiler site.

c. MESO and OPER AMV direct comparison

The statistical results described thus far indicate that OPER exhibit much closer agreement with profiler, with the OPER–profiler VRMS difference being ~3 m s^{-1} lower than MESO for the entire match database. In an effort to understand how and why MESO is observing differing flow than OPER, we will directly compare MESO and OPER for scenes where both vector types were present. AMVs are compared when vectors are within 50 km and 30 min of each other and have height assignments differing by less than 25 hPa. These criteria were selected to include the highest possible number of data matches within a reasonable temporal and spatial window. Figure 14 shows that the VRMS (DRMS) difference between vectors of the two processing types is 7.6 m s^{-1} (14.2°). These values are much higher than one might expect, given the identical or very similar scenes being evaluated within this 30-min time window.

To better understand the characteristics of these differences, we have closely examined animated *GOES-12* multispectral imagery in two situations: where vector differences between MESO and OPER are 1) less than 2 m s^{-1} and 2) greater than 10 m s^{-1}. Of the 247 total matches, 51 (39) AMV pairs agreed well (poorly). Imagery analysis reveals that the majority (75%) of the disparate AMV pairs originated from scenes with either multilayered or deep convective clouds. Pairs that exhibit good agreement originate from scenes with strato-

and altocumulus, "fair weather" cumulus, stratus, and thick cirrus clouds. When the two types of AMVs agree well, comparison to profiler indicates a 4.4 m s^{-1} VRMS difference for both processing schemes (not shown). When these AMVs have poor agreement, comparison with profiler provides an 11.5 m s^{-1} VRMS for MESO and 8.2 m s^{-1} for OPER (also not shown).

6. Discussion

The case study examples demonstrate that MESO can provide a wealth of realistic flow information over a broad geographic region in near–real time. These examples coupled with statistical validation results show that the impressive amount of flow information portrayed by the MESO comes with a cost though, namely increased spatial variability in the resulting AMV field. A subjective examination of the MESO and, to a lesser extent, OPER field in Figs. 3–5 and 7 reveals that significant variability can exist between closely spaced AMVs. This variability can hinder the effective use and interpretation of the MESO product, as high vector density coupled with natural spatial and vertical variability of the environmental wind field causes problems in understanding which vectors are most representative of the true flow.

Some degree of qualitative agreement is needed between nearby AMVs and the cloud pattern evolution in animated satellite imagery before a set of AMVs should
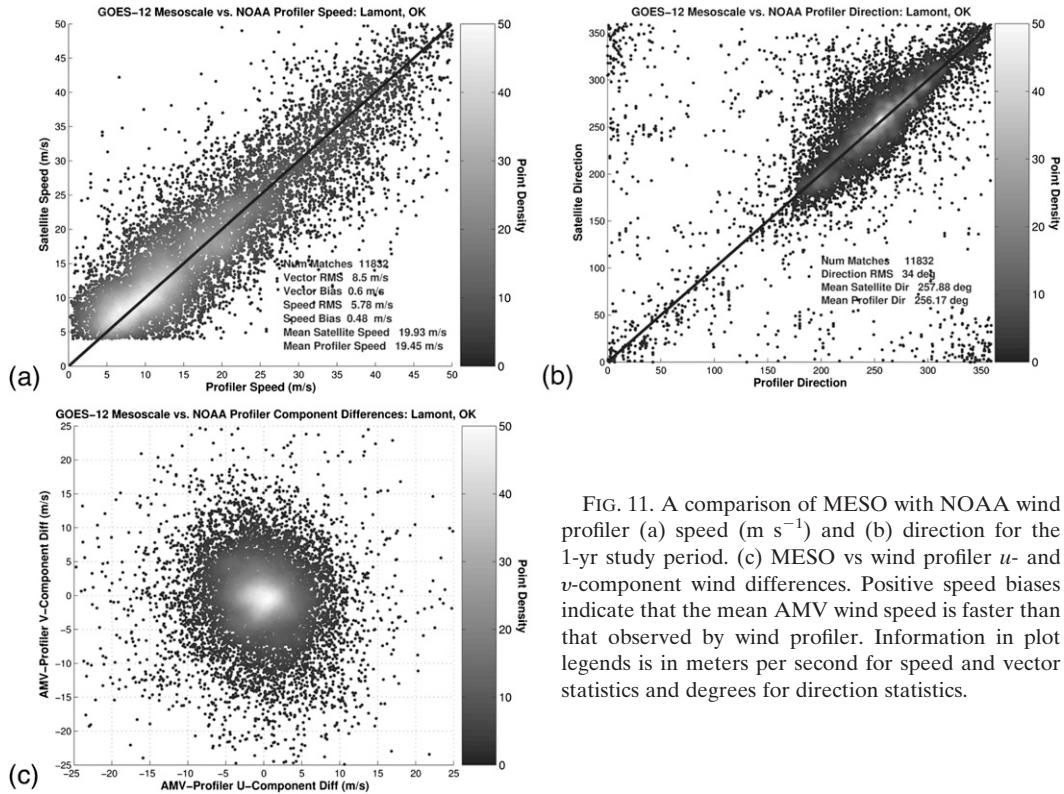
FIG. 11. A comparison of MESO with NOAA wind profiler (a) speed (m s^{-1}) and (b) direction for the 1-yr study period. (c) MESO vs wind profiler u- and v-component wind differences. Positive speed biases indicate that the mean AMV wind speed is faster than that observed by wind profiler. Information in plot legends is in meters per second for speed and vector statistics and degrees for direction statistics.

be accepted as realistic and accurate by a forecaster. As shown in Fig. 7a, northwest wind flow shown by numerous MESO and OPER depicted actual motions of a low cloud band as observed within animated *GOES-12* VIS imagery. The flow observed by collocated profiler data differs significantly from that portrayed in animated imagery, which would contribute a substantial degree of "error" to a statistical comparison. It is highly unlikely that this is the only case where apparent satellite-observed mesoscale cloud motions do not match the winds observed by the Lamont rawinsondes or profiler over the duration of the 1-yr statistical validation study period. Satellites simply observe cloud and water vapor motions and the relationship between this motion and the observed wind field is uncertain, especially for mesoscale gravity wave phenomena. Objective motion estimates from MESO for such phenomena can provide insight into atmospheric processes occurring at the mesoscale, which could have an impact within the forecast process. One should keep this in mind when assuming that the 8.5 m s^{-1} MESO–profiler VRMS is entirely a result of errant or "bad" vectors.

As the target box sizes are reduced significantly (relative to OPER) for MESO processing, one issue that may lead to increased error is related to limitations in VIS AMV height assignment accuracy for small

(<4-km width) cumulus clouds. VIS AMVs are generally assigned heights via the "IR window" technique, where the cloud-top 10.7-μm T_B is directly related to an NWP model temperature profile. When a VIS cloud feature does not fill an entire 4-km IR pixel, radiation from the earth's surface also reaches the satellite sensor, causing the IR T_B assigned to the VIS cloud to be
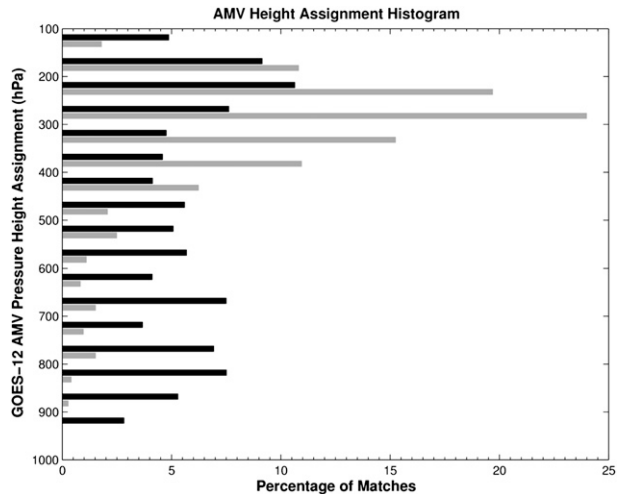

FIG. 12. A histogram of AMV to wind profiler match heights. MESO (OPER) matches are shown in black (gray).
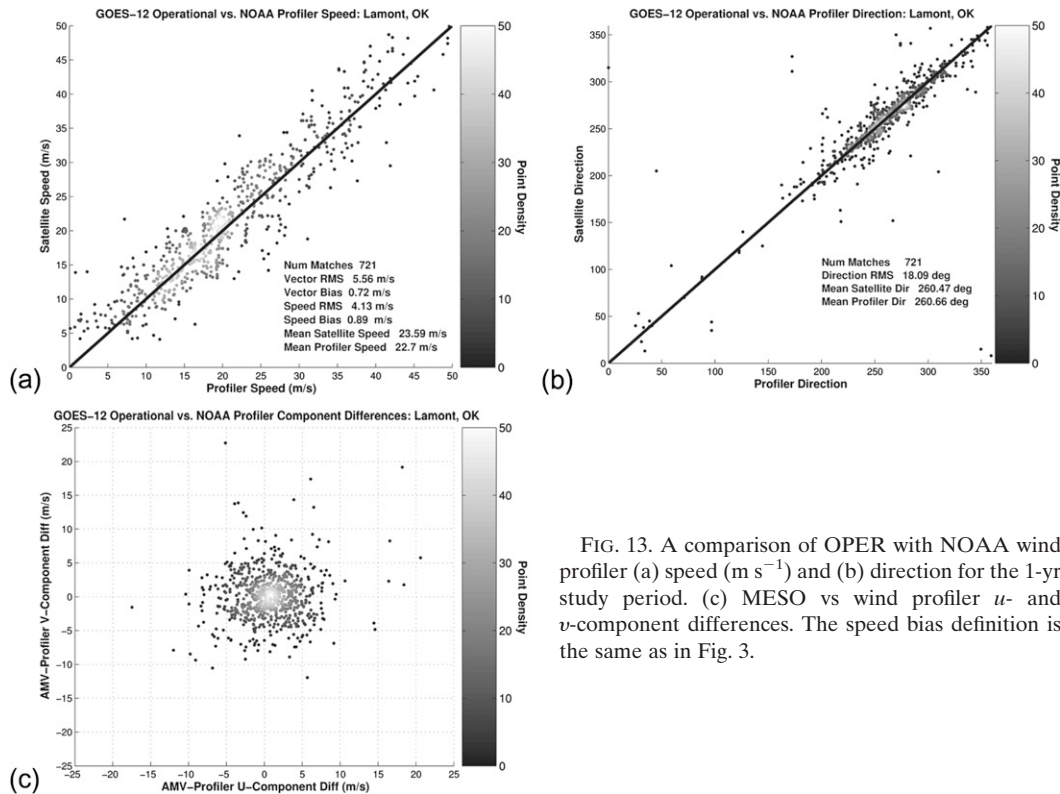
FIG. 13. A comparison of OPER with NOAA wind profiler (a) speed (m s^{-1}) and (b) direction for the 1-yr study period. (c) MESO vs wind profiler u- and v-component differences. The speed bias definition is the same as in Fig. 3.

warmer than its true cloud-top temperature. Therefore the cloud is assigned a height that is likely too low (Bedka et al. 2005), causing the AMV to be compared with flow from the wrong profiler and rawinsonde level. A small VIS cloud feature may be tracked perfectly in this case, but the resulting AMV could still carry an observation error as a result of this issue.

Differences in the composition and size of targets tracked by both MESO and OPER add further complication toward interpreting the differences between validation statistics, as motions from smaller scales are represented by MESO. Smaller 5 × 5 pixel MESO feature tracking boxes can capture detailed cloud and WV gradient features in a multilayer or deep convective cloud scene, compared to the OPER method where an ensemble of targets from differing levels can be contained in a 15 × 15 pixel box. Finescale motions of individual cloud elements are often not captured well in the synoptic-scale background wind analysis, but can

move faster than an ensemble of clouds. Since MESO are not forced to agree with a background wind analysis, these motions can often pass through the quality-control methods and be considered good vectors, provided their speed, directional, and spatial coherency are sufficient. An ensemble of features tracked by the OPER method may move differently across an image sequence than any single feature. An AMV from this ensemble motion will be considered a good vector if this movement fits well with the synoptic-scale background wind analysis and passes the QI checks. Thus, we end up with two disparate vectors, each of which represent some flow pattern observed within imagery and is therefore considered good within its respective processing framework.

7. Conclusions

The results of the statistical comparison between AMV and NOAA wind demonstrate that OPER exhibit

TABLE 4. A summary of match statistics for all MESO and OPER to wind profiler matches.

Comparison type	No. of vectors	Directional RMS (°)	Wind speed bias (m s^{-1})	Wind speed diff std dev (m s^{-1})	Wind speed RMS (m s^{-1})	Vector diff std dev (m s^{-1})	Vector RMS (m s^{-1})
All MESO vectors	11 832	34.02	0.48	5.76	5.78	8.03	8.50
All OPER vectors	721	18.09	0.89	4.02	4.13	5.00	5.56

TABLE 5. A summary of match statistics for all MESO and OPER to wind profiler matches, separated by AMV height assignment.

Comparison type	No. of vectors	Directional RMS (°)	Wind speed bias (m s^{-1})	Wind speed diff std dev (m s^{-1})	Wind speed RMS (m s^{-1})	Vector diff std dev (m s^{-1})	Vector RMS (m s^{-1})
MESO AMV							
VIS/IR/WV 1000–851 hPa	1227	51.10	−0.23	5.17	5.17	6.78	8.66
VIS/IR/WV 850–701 hPa	2108	40.09	1.54	4.97	5.20	7.53	7.91
VIS/IR/WV 700–401 hPa	3686	36.73	0.78	5.54	5.59	8.12	8.68
VIS/IR/WV 400–100 hPa	4811	21.10	−0.04	6.30	6.31	7.99	8.58
OPER AMV							
VIS/IR/WV 1000–701 hPa	27	30.53	−1.24	2.93	3.19	3.60	5.93
VIS/IR/WV 700–401 hPa	108	24.36	−0.57	4.03	4.08	4.67	5.42
VIS/IR/WV 400–100 hPa	586	16.01	1.25	3.98	4.17	4.73	5.57

closer agreement with ground-based observations than individual MESO for all height layers and AMV algorithm quality statistic values. Over a 1-yr period, the results show that MESO AMVs provide "good" wind estimates (less than 5 m s^{-1} VRMS differences) for 43% of the total vector matches (5087 out of 11 832 vectors), compared to 65% (469 out of 721 vectors) for the OPER method. Agreement between AMV and profiler is much closer though for higher QI statistic values and situations when MESO and OPER from near-identical scenes agree well. The MESO method provides a much more even vertical distribution of vectors compared to OPER, where the vectors were concentrated within the 400–100-hPa layer. Problematic scene types for both processing methods were deep convection, thin cirrus, and multilayered clouds.

Comparisons of collocated 6-min wind profiler and rawinsonde observations show VRMS differences of ~2.5 m s^{-1} within the 700–200-hPa layer, increasing to over 3.5 m s^{-1} within the stratosphere and near the mean top of the planetary boundary layer and earth's surface. Despite the presence of larger VRMS differences at some levels, the stability of the VRMS profile between 700 and 200 hPa in combination with the lack of significant outliers in the profiler–rawinsonde match database suggests that 6-min, ~400-MHz UHF wind

profiler data can be used to evaluate and better understand satellite AMV error characteristics.

Although individual MESO estimates may not always be as "accurate" as those depicted by the OPER method, the case event examples shown within this paper and other previous studies illustrate that the vastly increased MESO flow field density can benefit the diagnosis and forecasting of mesoscale weather phenomena in near–real time. Specifically, they provide useful indicators of the presence of low-level confluence, vertical wind shear, convective outflow, and mid- to upper-level divergence and vorticity patterns that are important in forecasting a variety of weather events. Comparisons to profiler observations for the 8 June 2005 event show that the apparent motion of a cloud band in animated satellite imagery differed significantly from perfectly collocated profiler observations, which calls into question the fundamental assumptions of AMV algorithms and validation studies that 1) clouds are nondeveloping features that are transported by the surrounding flow and 2) the satellite-observed cloud motions should match the actual wind flow at a single atmospheric level. To effectively use these AMV data for forecasting applications, forecasters should have some preliminary knowledge of the cloud pattern evolution within animated satellite imagery so they can

TABLE 6. A summary of match statistics for all MESO and OPER to wind profiler matches, separated by QI analysis score.

Comparison type	No. of vectors	Directional RMS (°)	Wind speed bias (m s^{-1})	Wind speed diff std dev (m s^{-1})	Wind speed RMS (m s^{-1})	Vector diff std dev (m s^{-1})	Vector RMS (m s^{-1})
MESO AMV							
0.50 ≤ QI score < 0.75	6216	39.74	0.17	5.97	5.95	8.19	8.98
0.75 ≤ QI score < 0.90	2625	30.79	0.71	5.65	5.69	8.01	8.33
0.90 ≤ QI score	2991	25.40	0.82	5.40	5.47	7.35	7.46
OPER AMV							
0.60 ≤ QI score < 0.75	105	29.07	0.54	5.34	5.37	6.69	7.44
0.75 ≤ QI score < 0.90	120	14.13	0.10	4.20	4.19	5.19	5.35
0.9 ≤ QI score	281	9.18	1.06	3.45	3.60	3.81	4.63

TABLE 7. A summary of statistics for MESO wind profiler matches for AMVs that were derived from thin cirrus and deep convective clouds and the statistical impact of removing these AMVs from the entire match database.

Comparison type	No. of vectors	Directional RMS (°)	Wind speed bias (m s^{-1})	Wind speed diff std dev (m s^{-1})	Wind speed RMS (m s^{-1})	Vector diff std dev (m s^{-1})	Vector RMS (m s^{-1})
MESO from thin cirrus	1804	27.57	1.47	6.23	6.40	7.76	8.89
MESO from deep convection	608	33.88	−1.10	7.01	7.10	9.14	10.19
All MESO with no thin cirrus	10 028	35.00	0.30	5.66	5.67	7.97	8.43
All MESO with no thin cirrus and deep convection	9420	34.98	0.39	5.55	5.56	7.89	8.30
All MESO with no thin cirrus, no deep convection, and QI > 90	2170	26.33	0.65	5.26	5.31	7.09	7.37

better differentiate useful AMV information from grossly errant flow estimates. One must also determine whether greater vector temporal update frequency and spatial flow detail (MESO method) or better relative accuracy (OPER method) will better suit his/her particular application when selecting an AMV processing scheme.

Assimilation of sets of high-quality MESO into a regional NWP model could provide positive impact on subsequent forecasts because of a more detailed representation of upper-air conditions at the mesoscale. As there would likely be mismatches between the atmospheric state represented by the conventional upper-air observing network and the MESO field, assimilation methods will need to be devised to optimize the retention of good information from MESO within an NWP model. Through the assimilation process, we will seek to gain an understanding of "value added" information provided by the MESO product to the initial analysis, considering the superior MESO density, greater overall MESO error, and NWP model horizontal resolution. Future work will focus on these topics as well as the development of an AMV quality-control scheme better

suited to operate on flow of the MESO product density. This new QC method could focus on combining closely spaced MESO to get an "ensemble average" observation, which should improve the overall accuracy and representativeness of the resulting AMV. Another QC approach could be to objectively identify scene characteristics and flag AMVs from the scene types shown to correspond with poor agreement to wind profiler in this study. Another future work item will be to further understand the AMV representativeness and height assignment uncertainty relative to high–vertical resolution ARM rawinsonde observations, which can help to determine the optimal way to assimilate and retain AMV information within NWP models.
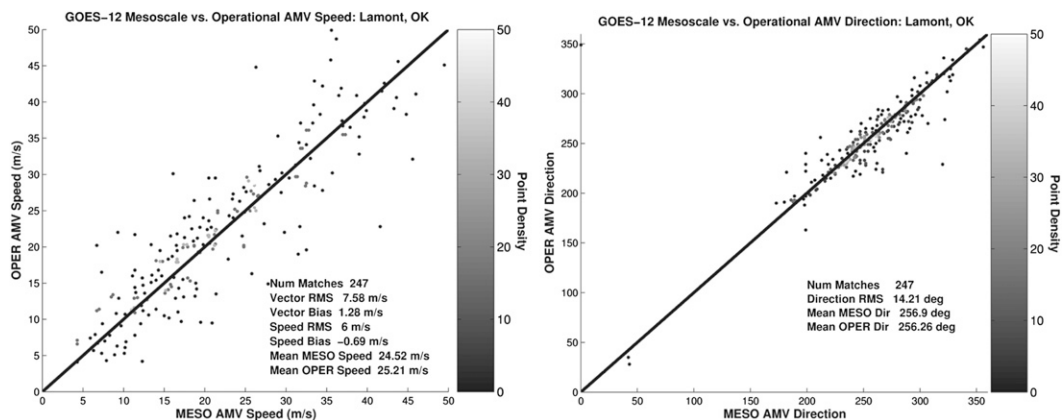
FIG. 14. A comparison between collocated MESO and OPER (a) speed and (b) direction for the 1-yr study period. A negative bias indicates that the MESO are slower than OPER on average.

REFERENCES

Bedka, K. M., and J. R. Mecikalski, 2005: Application of satellite-derived atmospheric motion vectors for estimating mesoscale flows. *J. Appl. Meteor.,* **44,** 1761–1772.

Bedka, S. T., W. F. Feltz, A. J. Schreiner, and R. E. Holz, 2005: Satellite-derived cloud top pressure product validation using aircraft based cloud physics lidar data from the ATReC field campaign. *Int. J. Remote Sens.,* **28,** 2221–2239.

Benjamin, S. G., and Coauthors, 2002: RUC20—The 20-km version of the Rapid Update Cycle. NOAA/NWS Tech. Procedures Bull. 490, NOAA/ERL Forecast Systems Laboratory, 30 pp.

Coulter, R., D. Hodlridge, and M. Ritsche, 2005: Balloon-Borne Sounding System (BBSS) Handbook. ARM, U.S. Department of Energy, DOE/SC-ARM/TR-029, 25 pp.

Dunion, J. P., and C. S. Velden, 2002: Application of surface-adjusted GOES low-level cloud-drift winds in the environment of Atlantic tropical cyclones. Part I: Methodology and validation. *Mon. Wea. Rev.,* **130,** 1333–1346.

Fisher, N. I., 1993: *Statistical Analysis of Circular Data*. Cambridge University Press, 277 pp.

Fujita, T. T., K. Watanabe, and T. Izawa, 1969: Formation and structure of equatorial anticyclones caused by large-scale cross-equatorial flows determined by ATS-I photographs. *J. Appl. Meteor.,* **8,** 649–667.

Goerss, J. S., C. S. Velden, and J. D. Hawkins, 1998: The impact of multispectral *GOES-8* wind information on Atlantic tropical cyclone track forecasts in 1995. Part II: NOGAPS forecasts. *Mon. Wea. Rev.,* **126,** 1219–1227.

Hayden, C. M., and R. J. Purser, 1995: Recursive filter objective analysis of meteorological fields: Applications to NESDIS operational processing. *J. Appl. Meteor.,* **34,** 3–15.

Holmlund, K., 1998: The utilization of statistical properties of satellite-derived atmospheric motion vectors to derive quality indicators. *Wea. Forecasting,* **13,** 1093–1104.

Jewett, C. P., 2007: Retrieval of convective momentum fluxes using geostationary satellite data. M.S. thesis, Atmospheric Science Dept., University of Alabama in Huntsville, 99 pp.

Kelly, G., T. McNally, J.-N. Thépaut, and M. Szyndel, 2004: OSEs of all main data types in the ECMWF operation system. *Proc. Third WMO Workshop on the Impact of Various Observing Systems on Numerical Weather Prediction,* Alpbach, Austria, WMO, 63–94.

LeMarshall, J. F., C. Spinoso, N. R. Pescod, and G. A. Mills, 1996: Estimation and assimilation of hourly high special resolution wind vectors based on GMS-5 observations. *Aust. Meteor. Mag.,* **45,** 275–284.

Lemone, M. A., 1973: The structure and dynamics of horizontal roll vortices in the planetary boundary layer. *J. Atmos. Sci.,* **30,** 1077–1091.

Leslie, L. M., J. F. LeMarshall, R. P. Morison, C. Spinoso, R. J. Purser, N. Pescod, and R. Seecamp, 1998: Improved hurricane track forecasting from the continuous assimilation of high quality satellite wind data. *Mon. Wea. Rev.,* **126,** 1248–1258.

Mecikalski, J. R., and K. M. Bedka, 2006: Forecasting convective initiation by monitoring the evolution of moving cumulus in daytime GOES imagery. *Mon. Wea. Rev.,* **134,** 49–78.

Negri, A. J., and T. H. Vonder Haar, 1980: Moisture convergence using satellite-derived wind fields: A severe local storm case study. *Mon. Wea. Rev.,* **108,** 1170–1182.

Nieman, S. J., W. P. Menzel, C. M. Hayden, D. Gray, S. T. Wanzong, C. S. Velden, and J. Daniels, 1997: Fully automated cloud-drift winds in NESDIS operations. *Bull. Amer. Meteor. Soc.,* **78,** 1121–1133.

Petersen, R. A., and K. M. Bedka, 2007: Determining the accuracy and representativeness of wind profiler data. Preprints, *11th Symp. on Integrated Observing and Assimilation Systems for the Atmosphere, Oceans, and Land Surface,* San Antonio, TX, Amer. Meteor. Soc., 6.10. [Available online at http://ams.confex.com/ams/pdfpapers/117332.pdf.]

Rabin, R. M., S. F. Corfidi, J. C. Brunner, and C. E. Hane, 2004: Detecting winds aloft from water vapor satellite imagery in the vicinity of storms. *Weather,* **59,** 251–257.

Rao, P. A., C. S. Velden, and S. A. Braun, 2002: The vertical error characteristics of GOES-derived winds: Description and experiments with numerical weather prediction. *J. Appl. Meteor.,* **41,** 253–271.

Rodgers, E., and R. C. Gentry, 1983: Monitoring tropical-cyclone intensity using environmental wind fields derived from short-interval satellite images. *Mon. Wea. Rev.,* **111,** 979–996.

Susko, M., and L. Herman, 1995: Comparison of satellite-derived wind measurements with other wind measurement sensors. *J. Spacecr. Rockets,* **32,** 564–566.

Velden, C. S., and K. M. Bedka, 2009: Identifying the uncertainty in determining satellite-derived atmospheric motion vector height attribution. *J. Appl. Meteor.,* **48,** 450–463.

——, C. M. Hayden, W. P. Menzel, J. L. Franklin, and J. S. Lynch, 1992: The impact of satellite-derived winds on numerical hurricane track forecasting. *Wea. Forecasting,* **7,** 107–119.

——, and Coauthors, 2005: Recent innovations in deriving tropospheric winds from meteorological satellites. *Bull. Amer. Meteor. Soc.,* **86,** 205–223.

Weber, B. L., and Coauthors, 1990: Preliminary evaluation of the first NOAA demonstration network profiler. *J. Atmos. Oceanic Technol.,* **7,** 909–918.

Xiao, Q., X. Zou, M. Pondeca, M. A. Shapiro, and C. S. Velden, 2002: Impact of *GMS-5* and *GOES-9* satellite-derived winds on the prediction of a NORPEX extratropical cyclone. *Mon. Wea. Rev.,* **130,** 507–528.

Yoe, J., M. Larsen, and E. Zipser, 1992: VHF wind-profiler data quality and comparison of methods for deducing horizontal and vertical air motions in a mesoscale convective storm. *J. Atmos. Oceanic Technol.,* **9,** 713–727.